AJEMA GLOBAL RESEARCH NETWORK

AMERICAN Journal of Engineering, Mechanics and Architecture
Volume 3, Issue 5, 2025 ISSN (E): 2993-2637

Analysis of Hall Sensor for Controlling the Speed of BLDC Motor Based E-Vehicle

G. Arun
Department of Electrical and Electronics Engineering, Dhaanish Ahmed College of Engineering, Chennai, Tamil Nadu, India
arun.g@dhaanishcollege.in

S. Kader Sultan, Mohammed Areeb, S. Seeni Ashik Rahman, K. Gopi
Department of Electrical and Electronics Engineering, Dhaanish Ahmed College of Engineering, Chennai, Tamil Nadu, India

Abstract: The subject of this project, which focuses on the electric vehicle's rear differential, is the examination of a high-performance brushless DC motor (BLDC) for an electric vehicle (EV) with Hall sensor control. Using a digital controller increases the drivsystem's flexibility. A DC-DC Bidirectional Dual Converter is implemented to supply BLDC motors utilizing Smart Power Modules. The suggested system is set to operate at the required speed and receives Hall sensor signals from the motor. The experimental findings confirm the efficacy of the created drive operation. A brushless DC motor is widely used in many different sectors and solves many of the issues a brushed DC motor has. Creating the BLDCM control system necessitates low cost, a fast development cycle, outstanding control algorithm performance, and dependable operation. The idea behind this project is the BLDC motor speed control for an electric vehicle. The use of a digital controller increases the drivsystem's flexibility. A Smart Power Module feeds The BLDC motor into the three-phase inverter. The experimental findings confirm the efficacy of the created drive operation.

Keywords: Microcontroller; Hall Sensors; Brushless DC Motor (BLDCM); DC-DC Bidirectional Dual Converter; Electric Vehicles (EV); Road Transportation.

Introduction

Electric vehicles are becoming increasingly significant because if electricity is produced from sources other than oil, it may be utilized to lessen the reliance on oil for transportation and reduce noise and pollution. Carbon emissions can also be decreased by using electric automobiles [8]. For electric vehicles to produce zero carbon dioxide emissions, energy must come from non-fossil fuel sources like nuclear and alternative energy [9]. In reality, as scarcity grows, prices will naturally soar to the point where using oil and other fossil fuels becomes unprofitable; as a result, oil will be saved as use declines [10]. Coal is one of the numerous fossil fuels that can be used to make oil [11]. In the past, oil produced in this manner was considered around 10% more expensive, but given the current oil prices, coal production is beginning to become profitable [12]. Though it remains a limited resource, coal is more plentiful than oil and can last more than a century. Concerns about global warming are still growing [13]. Burning fossil fuels releases carbon dioxide, which is blamed for causing global warming [14]. This

phenomenon is thought to be the cause of numerous issues, such as rising sea levels and climate change, which have the potential to devastate coastal towns across the globe completely [15].

Whereas road transportation has only recently advanced so that automakers are beginning to mass-produce electric automobiles, electric trains are well-developed and extensively utilized [16]. Electric road vehicles are not as common as small electric vehicles utilized in specialized sectors, such as golf buggies, electric bicycles, and electric carriages [17]. Compared to internal combustion (IC) engine vehicles, which typically have a much longer range and are very simple to refuel, electric road vehicles have not had the same level of success [18]. Understanding the fundamentals behind the design of electric vehicles and the pertinent technological and environmental challenges is crucial [19]; these topics will be covered in detail in the upcoming chapters.

Technology of Electric Motors

Electric motor technology encompasses a wide range of fields, including electronics, materials, sensors, control technologies, and machine architectures [20]. Developing a high-performance drive requires the creation of suitable converters and control algorithms for different types of motors [21]. Key components of various converter designs include the converter's efficiency and dynamic reactivity [22]. The reason converters have low power loss is because they are very efficient [23]. Because of this characteristic, DC drive systems that use a three-phase power system can remove the third harmonic and all of its associated components from the output [24]. In a three-phase system, the ripple voltage is much lower than in a one-phase one [25].

Current events are marked by numerous crises, such as excessive oil costs and outdated designs. So, in politically stable places, there is a hunt for more efficient road automobiles that may be sourced from environmentally good sources [28]. The development of electric cars is a direct outcome of this. Electric vehicles (EVs) such fuel cell EVs, plug-in hybrid EVs, hybrid EVs, and battery EVs are increasingly common in the transportation sector [29]. The impact of rapid and intelligent charging on the electrical grid, as well as the longevity and degradation of batteries, is a topic of conversation in light of the growing number of electric vehicles [27].

The DC voltage is sourced by most EVs. Direct DC use is preferable since it does away with the requirement for additional converter hardware [30]. The charger's features and the charging infrastructure have an impact on the batteries' performance, along with the batteries' types and designs [31]. Fuel cell hybrid electric vehicles (FCHEVs) combine high-energy batteries with high-power-density ultra-capacitors to create compact, lightweight, efficient, and powerful electric vehicles [32]. The amount of energy required to minimise the volume and mass of a battery is a common metric for evaluation [26]. The functions and conditions that the EV motor drive system must handle are as follows:

- High torque-producing capacity;
- High acceleration;
- High power intensity;
- High torque when running at slow speeds with high efficiency (to run on any terrain and in harsh environments);
- High efficiency concerning the regenerative braking capacity (for battery charging)

Electric Vehicle Types: EV Architecture

As illustrated in Figure 1.1, the idea of a battery electric vehicle (EV) is fairly straightforward. The vehicle comprises an electric motor, a controller, and a battery for energy storage [33].

The Electric Hybrid Car with An IC Engine

A hybrid car can have two or more power sources, which leads to an enormous variety of possible configurations. The most popular hybrid car models combine an internal combustion engine, battery, electric motor, and generator.

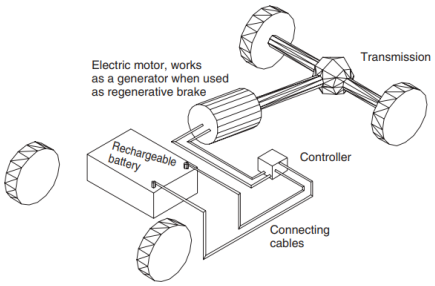

Figure 1.1: Electric Car with Rechargeable Batteries

Figures 1.2 and 1.3 depict the two fundamental configurations for hybrid vehicles: the parallel hybrid and the series hybrid. One or more electric motors powered directly by the battery, the generator unit powered by the IC engine, or both power the vehicle in a series hybrid configuration [34]. The vehicle in a parallel hybrid can be powered by the engine directly through a transmission system, by one or more electric motors connected directly to the wheels through the transmission, or by the electric motor and the internal combustion engine simultaneously [35]. The hybrid system that operates in parallel has various configurations.

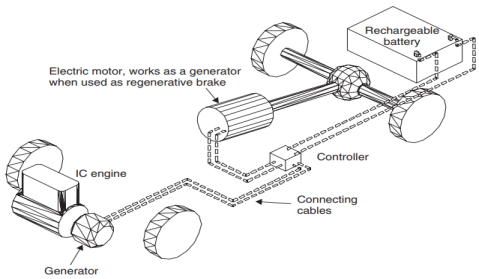

Figure 1.2: Rechargeable HybriVehicles' Series Hybrid Vehicle Arrangement.

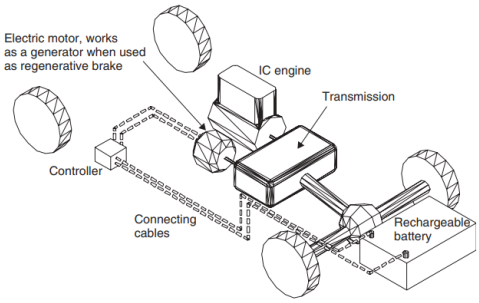

Figure 1.3: Layout of a Parallel Hybrid Car.

Literature Survey

A high-efficiency speed control scheme for brushless DC motors employs Hall-effect sensors to detect rotor position and generate commutation signals. This approach uses trapezoidal pulse-width modulation to drive the three-phase windings, while a proportional-integral controller regulates rotational speed. Experimental findings demonstrate that incorporating PI feedback significantly improves stability and accuracy, reducing speed fluctuations under varying load conditions and ensuring tight speed regulation compared to open-loop or sensorless techniques [1].

A robust fault-tolerant system addresses failures in Hall-effect position sensors within brushless DC motor drives. The method continuously monitors line voltage harmonics via discrete Fourier analysis to detect sensor malfunctions. Upon fault identification, an expert logic module

synthesizes replacement commutation signals, enabling uninterrupted motor operation. Validation through simulation and experimental benchmarking confirms that this lightweight algorithm restores proper sequencing without imposing heavy computational demands, allowing seamless integration into existing control firmware [2].

A reconfigurable fault-tolerant control architecture for electric vehicle motor drives ensures reliable operation when voltage sensors degrade. Under standard conditions, the system employs direct torque control for rapid torque response. If a voltage sensor fault is detected, control automatically transitions to field-oriented control, maintaining smooth torque production and stable speed. Simulation results verify that the switchover preserves drive performance while avoiding vehicle control interruptions, demonstrating a practical solution for enhancing safety and dependability in electric propulsion applications [3].

An electronic control unit design integrates a real-time network protocol with a proportional-integral controller to manage a three-phase brushless DC motor. Optimization of PI gains via a multiobjective genetic algorithm ensures balanced speed regulation and minimal torque ripple. Hardware-in-the-loop validation using a networked simulation environment confirms that the controller autonomously schedules insulated-gate bipolar transistor switching sequences over a vehicular communication bus. Results indicate enhanced dynamic response and robustness, validating the ECU's architecture for use in low-pollution transportation systems [4].

A locally developed motor controller for three-phase brushless DC tricycle drives converts battery DC voltage into synchronized AC waveforms for each motor phase. PCB-based implementation and software simulation compare performance against an imported controller, revealing comparable efficiency and dynamic response. Laboratory tests measure torque output, current draw, and speed stability under nominal load, confirming that the indigenous design meets industry benchmarks. The project underscores the potential for cost-effective domestic manufacturing of key electric vehicle components without compromising reliability [5].

A compact hardware system controls both speed and angular position of a gearbox-coupled brushless DC motor by leveraging internal Hall sensors. A microcontroller reads position feedback and user inputs via serial communication, then computes velocity and position setpoints in real time. The control firmware issues commutation sequences and torque commands, achieving fine resolution in shaft movement with a ten-to-one reduction ratio. This closed-loop solution matches or exceeds the precision of conventional stepper- or servo-motor assemblies in low- to medium-precision automation tasks, offering a simpler and more economical alternative [6].

An evaluative study compares various electric vehicle propulsion motor technologies, analyzing parameters such as efficiency, torque-to-weight ratio, thermal performance, and control complexity. Assessments cover DC, induction, and brushless DC machines, highlighting the latter's superior efficiency and maintenance profile. The review also examines driver electronics, including control algorithms and inverter topologies, to determine optimal pairings for different vehicle classes. Findings guide designers in selecting the most suitable motor-drive combinations based on performance requirements, cost constraints, and application-specific criteria [7].

BLDC Motor

A Brief Overview of BLDC Motors

As the name suggests, BLDC motors are electronically commutated rather than using brushes for commutation. Compared to brushed DC and induction motors, BLDC motors offer several benefits. Several of these include:

- Improved torque versus speed characteristics
- Extremely dynamic response
- Extended speed ranges;

- Noiseless operation;
- Extended working life;

Additionally, the torque provided to the motor's size ratio is higher, which makes it helpful in applications where weight and space are important considerations. In this application note, we will detail the design, operation, features, and common uses of BLDC motors.

The BLDCMMotor's Construction and Operation Principle

Synchronous motors include BLDC motors. This indicates a frequency difference between the magnetic fields produced by the rotor and the stator. The "li" "hat induction motors typically encounter is not experienced by BLDC motors. BLDC motors are available in single-, two-, and three-phase variants. Thesstator's winding count is the same as that of its kind. Three-phase motors are the most common and are extensively utilized. 3-phase motors are the subject of this application notice [36].

Stator

A BLDCmmotor's stator comprises stacked steel laminations with windings positioned in the axially cut slots along the inner periphery (as illustrated in Figure 3.3). Conventionally, the stator is similar to an induction motor, but the windings are arranged differently [37]. The majority of BLDC motors have three stator windings connected in a star pattern, each of which is made up of multiple coils that are connected to form a winding; one or more coils are positioned in the slots and are connected to form a winding; these windings are then distributed over the stator periphery to form an even number of poles [38].

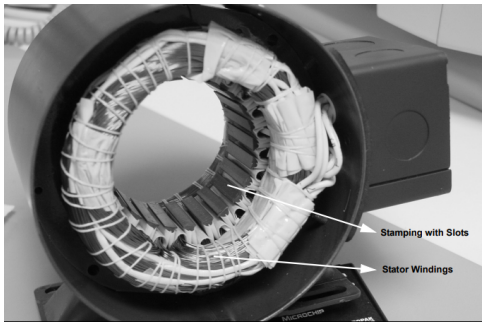

Figure 3.1: Stator of a BLDC Motor

Trapezoidal and sinusoidal motors are the two varieties of stator windings. To provide the various forms of back Electromotive Force (EMF), this difference is based on the connecting of coils in the stator windings [39]. As their names suggest, the back EMF of a sinusoidal motor is sinusoidal, while the back EMF of a trapezoidal motor is trapezoidal, as Figures 3.1 and 3.2 illustrate [40]. For each type of motor, the phase current varies in a trapezoidal and sinusoidal manner in addition to the back EMF [41].

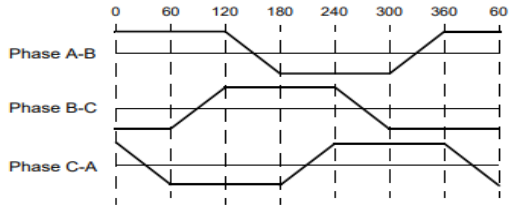

Figure 3.2: Trapezoidal Back Emf

Because of this, a sinusoidal motor produces torque more smoothly than a trapezoidal motor [42]. The distribution of the coil on the stator periphery necessitates additional winding interconnections for sinusoidal motors, which increases the copper intake by the stator windings and carries an additional cost [43].

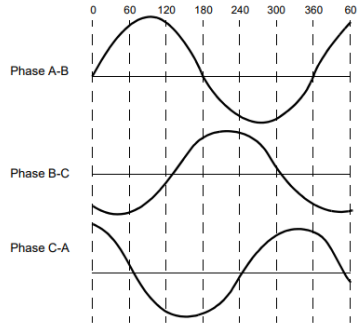

Figure 3.3: Sinusoidal Back Emf

3.2.2. Motor

The rotor's pole pairs can range from two to eight with alternating North (N) and South (S) poles. It is composed of permanent magnets [44]. The right magnetic material is selected based on the necessary magnetic field density to create the rotor [45]. Permanent magnets are often made with ferrite magnets. Magnets made of rare earth alloys are becoming increasingly popular as technology develops [46]. Although ferrite magnets are less expensive, their low flux density for a given volume is a drawback [47]. On the other hand, the alloy material allows the rotor to compress deeper for the same torque because of its high magnetic density per volume [48]. Additionally, these alloy magnets increase the torque output for a motor of the same size while improving the size-to-weight ratio [49]. Magnets made of rare earth alloys include neodymium (Nd), samarium cobalt (SmCo), and neodymium, ferrite, and boron (NdFeB) [50]. Research is always done to increase the flux density and compress the rotor even more. Figure 3.4 depicts cross-sections of several magnet setups in a rotor.

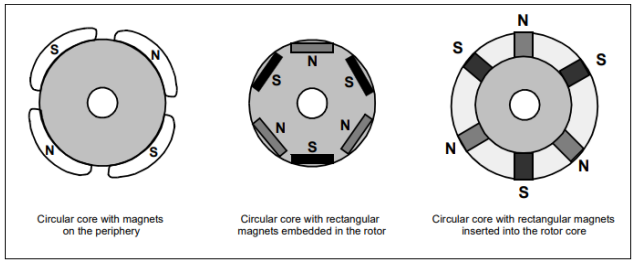

Figure 3.4: Cross Sections of a Rotor Magnet

3.3. Hall Sensors

Unlike a brushed DC motor, a BLDCmmotor's commutation is electronically controlled. To rotate the BLDC motor, the stator windings must be activated sequentially [51]. Knowing the rotor position is critical to determining which winding will be activated after the energizing procedure. Hall effect sensors implanted in the stator detect the territory's location.

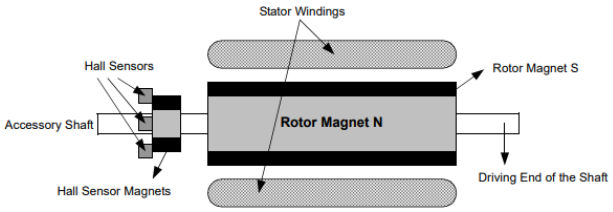

Figure 3.5: BLDC Motor Transverse Section

Figure 3.5 shows the cross-section of a BLDCmmotor with a rotor that switches between permanent magnets of the N and S types. The stationary part of the motor has hall sensors integrated into it [52]. Imbedding the Hall sensors into the stator is a complex procedure since they must be perfectly aligned with the rotor magnets for the rotor position calculation to be accurate [53]. To facilitate the attachment of the Hall sensors to the stator, certain motors may include both the usual rotor magnets and Hall sensor magnets [54]. These are scale

representations of the rotor on a lesser scale [55]. At each rotation of the rotor, the Hall sensor magnets exert the same force as the main magnets [56]. On the end that isn't being driven, you'll usually find hall sensors linked to the enclosure cap, which is mounted on a PC board [57]. To get the most out of their Hall sensors, users can adjust the whole system so that they line up with the rotor magnets. The location of the Hall sensors determines the sort of output that is produced [58]. A phase shift of 60 or 120 degrees is possible with the Hall sensors [59]. The maker of the motor uses this information to establish the proper commutation sequence for controlling the motor [60]. You may find more details about the commutation sequence and see an example of Hall sensor signals under the "commutation Sequence" section [61].

Theory of Operation

Each commutation sequence consists of turning on one winding (bringing current into it), turning off the other (taking current out of it), and then turning on the third (not turning it on). Torque is produced when magnetic fields interact with permanent magnets [62]. In a perfect world, the maximum torque would be generated at a right angle to the other field and would diminish as the fields moved in tandem [63]. In order for the motor to continue turning, the windings' magnetic field must change orientation as the rotor approaches the stator's field [64]. The "ix-Step Commutatio" sequence describes the process of energising the windings. For further information and a six-step commutation example, go to the "commutation Sequence" section. A power supply is necessary for the Hall sensors [65]. A voltage of 4–24 volts is possible. A current of 5 to 15 milliamperes may be necessary [66]. For the precise ratings of the Hall sensors' voltage and current, please consult the technical specifications of the monitor before building the controller [67]. The output of a Hall sensor is usually of the open-collector variety [68]. On the controller side, a pull-up resistor might be necessary.

Torque/Speed Characteristics

The torque/speed relationship is illustrated in Figure 3.6. The peak torque (TP) and rated torque (TR) are the two torque metrics that define a BLDC motor. Appendix A, "Typical Motor Technical Specification," contains a comprehensive list of parameters [69]. It is possible to load the motor to its rated torque during continuous operations [70]. A BLDC motor's torque is constant up to the given speed, as mentioned above. There is a decrease in torque as the motor is used at speeds above 150% of its rated speed. Torque values greater than the specified value are required for applications involving rapid starts and stops as well as rotational reversals while the motor is loaded [71]. Especially when starting from a stop or accelerating, this requirement is there for a short while [72]. To overcome the inertia of the load and the rotor, more torque is required at this moment [73]. In order for the motor to produce more torque between its maximum and peak speeds, it must follow the speed torque curve [74]. Refer to the "Electing a Suitable Motor Rating for the Application" section for guidance on how to select these attributes for a particular task [75].

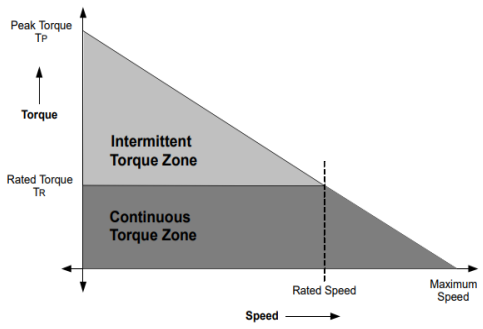

Figure 3.6: Torque/Speed Characteristics

Comparing Brushless DC Motors to Other Motor Types

BLDC motors have numerous advantages over brushed DC motors and induction motors. Brushless motors require less maintenance and last longer than brushed DC motors. BLDC motors have a higher output power per frame size than brushed DC and induction motors. Because the rotor comprises permanent magnets, it is less inert than other motors [76]. This enhances acceleration and deceleration characteristics, shortening the operating cycle. Nonetheless, the "rushe" DC motor is the most basic type of electric motor—at least in terms of comprehension. Portable tools, toys, electrically controlled car windows, and tiny household appliances like hair dryers—even ones that run on the AC mains—all make extensive use of this kind of motor.1. Though the other motor types discussed later in this chapter are becoming more popular for this use, it is still utilized as a traction motor [77-82]. The brushed DC motor is a good place to start since it is quite common and makes it easier to understand the most significant challenges in electric motor management. The following are the most significant of these:

- To prevent the magnet's magnetic field from being weakened by covering a wide air area, the revolving wire coil, also known as the armature, is wound around a piece of iron.
- More than one coil will be employed, increasing the time a current-carrying wire spends close to the magnets. This indicates multiple commutator segments, one for each coil, rather than two half-rings.
- Each coil will have many wires to increase the torque (more wires, greater force).

Computation Sequence

Figure 3.7 depicts an example of Hall sensor signals concerning the back EMF and phase current. Figure 8 depicts the switching sequence that should be used concerning the Hall sensors. The sequence numbers in Figure 3.7 match those in Figure 3.8. Every 60 degrees of electrical rotation, one of the Hall sensors changes state. Given this, completing an electrical cycle requires six steps. The phase current switching should be updated every 60 electrical degrees in synchronous operation.

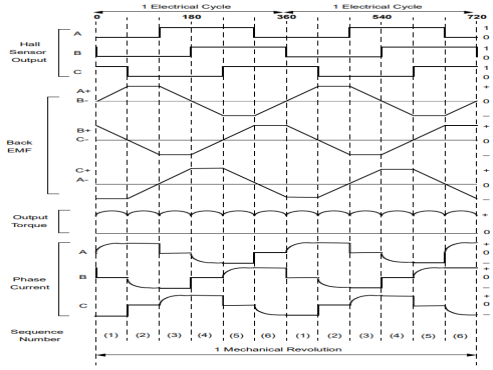

Figure 3.7: Hall Sensor Signal, Back Emf, Output Torque, and Phase Current

However, one electrical cycle may not be equivalent to a full mechanical revolution of the rotor. The rotor pole pairs dictate the electrical cycles required for a mechanical revolution. Each pair of rotor poles completes one electrical cycle. So, the number of electrical cycles/rotations equals the number of rotor pole pairs. Figure 3.9 is a block diagram of the controller used to drive a brushless DC motor. The PIC18FXX31 microprocessor controls the power switches Q0–Q5. Depending on the motor voltage and current specifications, these switches may be MOSFETs, IGBTs, or basic bipolar transistors.

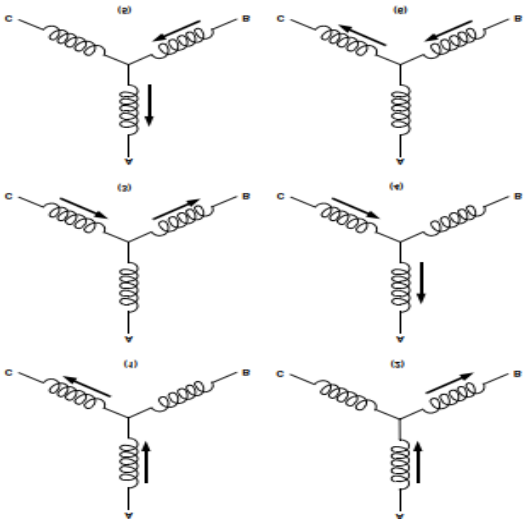

Figure 3.8: Winding Energizing Sequence concerning the Hall Sensor

Tables 3.3 and 3.4 demonstrate the order in which these power switches should be switched based on the Hall sensor inputs A, B, and C. Table 3.3 shows the clockwise rotation of the motor. This is an example of Hall sensor signals with a 60-degree phase shift relative to each other.

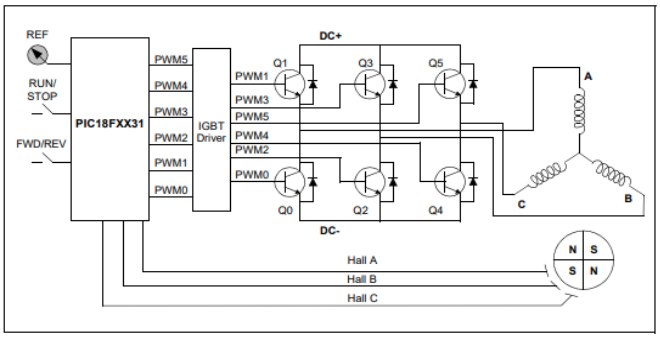

Figure 3.9: Control Block Diagram

Figure 3.9 shows that the motor will operate at its rated speed if the signals represented by PW Mx are turned on and off in the correct order. Assuming the DC bus voltage is equal to the rated voltage of the motor plus any losses across the switches, this is the case. Pulse Width Modulated (PWM) impulses with a much higher frequency than the motor's are required to alter the speed. A good rule of thumb is to set the PWM frequency ten times higher than the maximum frequency that the motor can handle. Altering the PWM duty cycle within the sequences lowers the speed by decreasing the average voltage supplied to the stator. One further perk of pulse width modulation (PWM) is that it allows you to control the motor by limiting the percentage of the duty cycle that corresponds to the motor-rated voltage, which is useful when the DC bus voltage is much greater than the motor-rated voltage. By altering the PWM duty cycle, the controller may connect motors with different rated voltages and ensure that the average voltage output matches the motor's rated voltage. Methods of control differ. So, let's say the microcontroller has restricted PWM signals. In that instance, the duty cycle of the PWM can control the appropriate lower switch, and the relevant sequence can be used to turn on the higher switches. To establish a reference speed, a potentiometer is connected to the analog-to-digital converter channel, as shown in Figure 3.9. Use this input voltage to determine the pulse width modulation duty cycle.

Table 3.3: Sequence for Rotating the Motor in a Clockwise Direction When Viewed from Non-Driving End

Sequence	Hall Sensor Input			Active PWMs		Phase Current		
	A	B	C			A	B	C
1	0	0	1	PWM1(Q1)	PWM4(Q4)	DC+	Off	DC-
2	0	0	0	PWM1(Q1)	PWM2(Q2)	DC+	DC-	Off
3	1	0	0	PWM5(Q5)	PWM2(Q2)	Off	DC-	DC+
4	1	1	0	PWM5(Q5)	PWM0(Q0)	DC-	Off	DC+
5	1	1	1	PWM3(Q3)	PWM0(Q0)	DC-	DC+	Off
6	0	1	1	PWM3(Q3)	PWM4(Q4)	Off	DC+	DC-

Closed-Loop Control

The speed can be managed in a closed loop by measuring the motor's speed. The error between the set speed and the actual speed is determined. A Proportional, Integral, and Derivative (P.I.D.) controller can amplify the speed error and modify the PWM duty cycle dynamically. Hall signals can measure speed feedback at a minimal cost and with low resolution. To count the duration between two Hall transitions, use a timer from the PIC18FXX31. With this count, the motor's true speed can be computed. An optical encoder can be installed on the motor for high-resolution speed measurements, producing two signals with a 90-degree phase difference.

Back emf equation=(E) □ N*l*r*B*□

The rotor magnetic field and the stator windings' number of spins don't change after the motor is designed. Back EMF is solely determined by the rotor's angular velocity, or speed, and it grows in tandem with the rotor's speed. The back EMF constant, a parameter in the motor technical specification, can be used to calculate back EMF at a specified speed. One can compute the potential difference across a winding by deducting the supply voltage from the back EMF measurement. The motor's back EMF constant is engineered so that, when operating at the rated speed, the motor will have enough potential difference between the supply voltage and back EMF to draw the rated current and produce the rated torque. A drooping torque curve can be caused by a motor driven faster than its rated speed because of a significant rise in back EMF, which lowers the potential difference across the winding and draws less current. When the supply voltage equals the total of the motor's losses, and the back electromagnetic field, the torque and current are zero, the final point on the speed curve.

BLDC Motor Sensorless Control

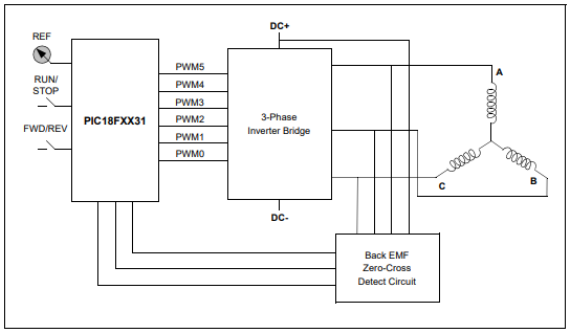

Figure 3.10: Block Diagram of Sensorless Control

Thus far, we have observed commutation based on the Hallssensor's indication of the rotor position. One might use the back EMF signals rather than Hall sensors to communicate BLDC motors. Figure 3.7 illustrates the interaction between the Hall sensors and back EMF in response to the phase voltage. As we have seen in previous sections, every commutation sequence has one winding energized positively, the second negative, and the third left open. As seen in Figure 3.7,

when the voltage polarity of the back EMF crosses from a positive to a negative or from a negative to a positive condition, the Hall sensor signal changes. Ideally, this occurs when the back EMF zero-crosses, but there will be a delay because of the winding characteristics. The microcontroller should adjust for this delay. Figure 10 displays a block diagram for BLDC motor sensor-less control.

Extremely low speeds are another factor to take into account. Back EMF would be at a very low amplitude to detect zero-crossing at a very low speed because it is related to the rotation speed. Start the motor in the open loop from a standstill. After building up enough back EMF to detect the zero-cross point, switch the control to the back EMF sensing. From the motor's back EMF constant, one can determine the lowest speed at which back EMF is perceptible. This commutation method allows the removal of the Hall sensors and the magnets for the Hall sensors in some motors. This lowers the cost and streamlines the motor's construction. This is useful if the motor works in an oily or dusty environment where the Hall sensors must be cleaned periodically to function properly. If the motor is installed in a less accessible area, the same rules apply.

Analysis of Hall Sensor

The software shown in Fig.4.1 flow diagram is organized into two threads, one for each completed primary function. Two independent timers regulate the threads, with the motor control thread receiving the highest priority. The simulation considered the commutation table shown in Fig 4.3. Fig.4.4 displays the Simulink model. The simulation's three outcomes are the stator current waveform, rotor speed, and electromagnetic torque ripple. The plots in Fig4.2. Display these findings.

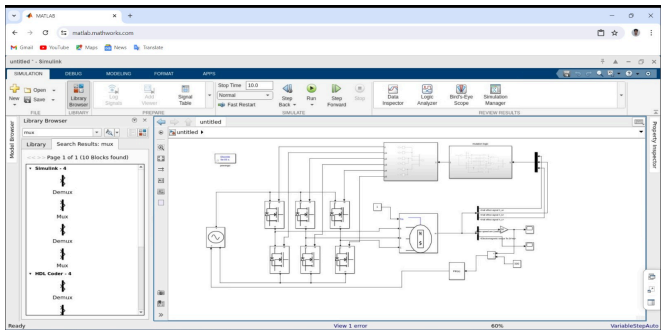

Figure 4.1: Simulink Motor Model for Suggested Configuration

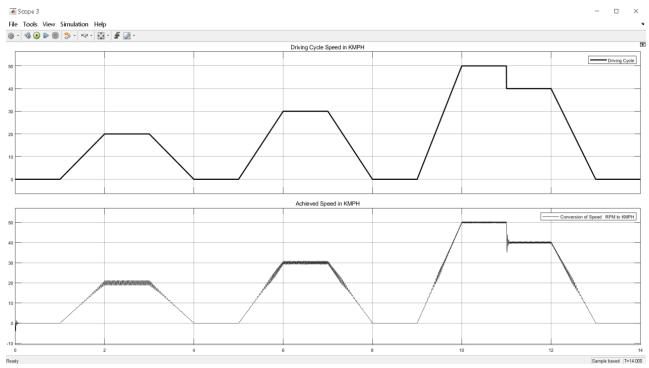

Figure 4.2: System Simulation Results for Driving Cycle Speed and Achieved Speed

The A/D converter reads the desired speed from an external potentiometer to create a software value called Reference Speed. The measured speed is then used to adjust the motor's output voltage based on the difference between the desired and measured speeds.

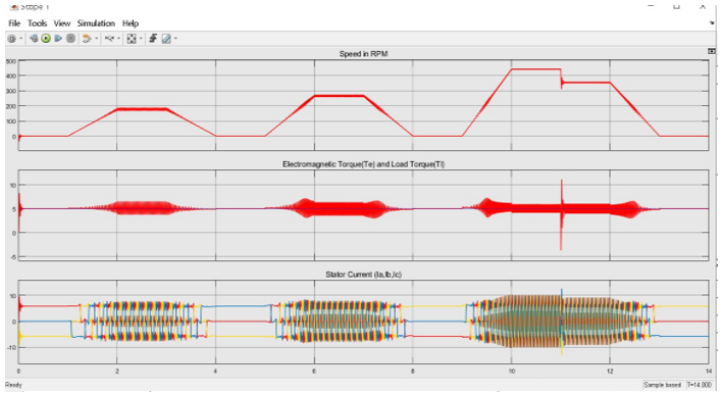

Figure 4.3: Displays the Simulation Results of the System for Speed, Electronic Torque, and Stator Current

Figure 4.1 shows the waveforms of the hall sensors A and B, and Figure 4.4 depicts several PWM pulses obtained straight from the Digital Storage Oscilloscope. Figures depict the stator currents for phases R, Y, and B.

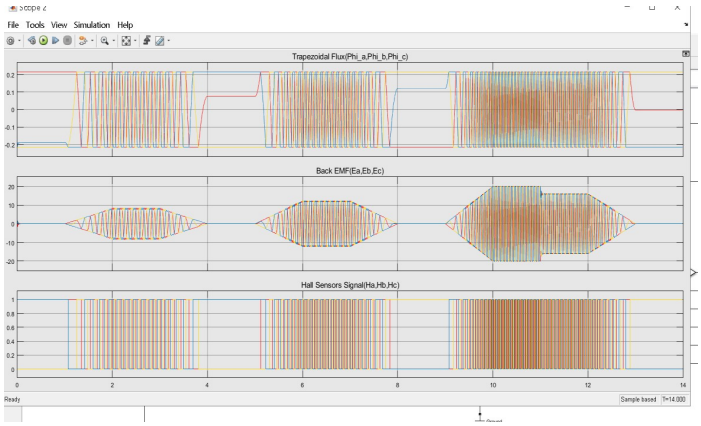

Figure 4.4: Simulation Results of the System for Trapezoidal Flux, Back Emf, and Hall Sensors

Block Diagram of the Control System

The BDLC motor uses Hall sensors to determine the rotor's position. Position information requires three sensors. It is feasible to obtain six different commutation sequences with three sensors. The Hall sensor method arranges three Hall sensors 120 degrees apart inside the motor. Depending on the polarity of the magnetic pole nearby, each Hall sensor outputs either a high or low value. The analysis of the three Hallssensors' outputs yields the rotor position. The three phases of the motor's voltage are altered based on the output from the hall sensors. One benefit of commutation based on Hall sensors is the straightforward control algorithm. Low-speed operation of the motor is also possible with Hall sensor-based commutation. Single-current operation is required for BLDC motor control. For this reason, it is not advisable to install a current sensor on each motor phase; instead, one sensor at the line inverter input will be enough to regulate each phase's current. Sensors placed on the ground line do not require insulated systems.

A microprocessor controls the torque and speed of motors. Completing the algorithms that produce Pulse Width Modulated (PWM) outputs for motors requires significant computer resources. One may easily adjust the motor's speed by changing the voltage across it. Changing the duty cycle of the PWM signal makes it simple to vary the motor voltage when utilizing PWM outputs to operate the three-phasebbridge's six switches. It is possible to adjust the three-phase BLDC speed using both closed-loop and open-loop topologies. By directly adjusting the duty cycle of the PWM signal that steers the motor-drive circuitry, open-loop control allows for precise motor speed control.

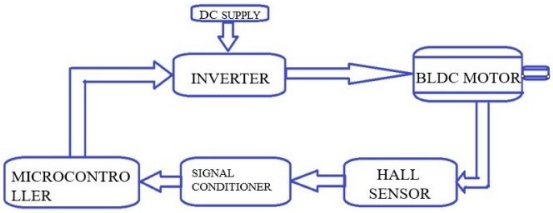

Figure 5.1: Block diagram of BLDC drive system

In the half bridges of the motor-drive circuit, the duty cycle of the PWM signal regulates the power switches ON times, which in turn regulates the average voltage applied across the motor windings. Through direct control of the duty cycle of the PWM signals that drive the motor-drive circuitry, closed-loop control modifies the motor's speed. The primary distinction between the two control systems is that the closed-loop control updates the PWM duty cycle and the motor speed by considering both the actual motor speed (feedback to the controller) and the speed control input in the open-loop control. The most popular application for a P.I.D. controller is a feedback controller. It is a widely used closed-loop control system. Tracking the interval between consecutive Hall events—a portion of the motor's mechanical cycle—allows one to determine the real motor speed.

Methodology

Implementation

A rotor position sensor is necessary for PM motor drives to correctly carry out phase commutation and/or current regulation. PMAC motors require a continuous flow of position data. Hence, a high-resolution position sensor such as a shaft encoder or a resolver is usually employed. Hall-effect sensors are often inexpensive because they only need to know the six-phase-commutation instants in an electrical cycle for BLDC motors. The measurement of motor position and speed has also made considerable use of accelerometers and electromagnetic variable reluctance (VR) sensors. In actuality, angular motion sensors that rely on magnetic field sensing principles are unique due to their numerous intrinsic benefits and detecting advantages.

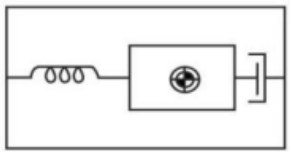

Figure 6.1: Accelerometer

An electromechanical instrument known as an accelerometer is used to detect acceleration forces associated with the freefall phenomenon. Numerous kinds of information are accessible to feel, such as location, vibration, shock, and the amount and direction of acceleration as a vector quantity. The most popular design is based on a fusion of Hooke's law of spring action and Newton's equation of mass acceleration. Among the numerous other types are potentiometric, linear variable differential transformers (LVDT), variable capacitance, piezoelectric, and piezo-resistive. Since the MEMS accelerometer is silicon micro-machined, integrating it with the signal processing circuitry is simple.

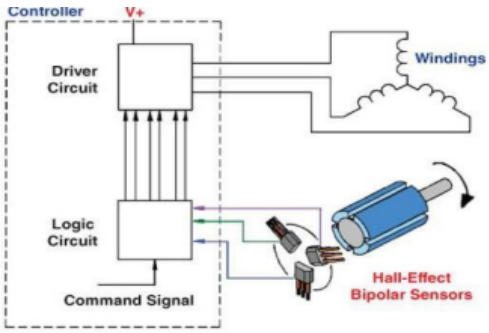

Figure 6.2: BLDC Motor with Hall Sensor

These devices are based on the Hall-effect hypothesis, which posits that when an electric current-carrying conductor is placed in a magnetic field, the charge carriers tend to be pushed to one side of the conductor by the transverse force of the magnetic field. There will be a detectable voltage between the two sides of the conductor when a build-up of charge at their respective sides balances this magnetic influence. The term "all-effect" refers to this detectable transverse voltage.

Experimental Set Up

The BLDC motor specifications are shown in Table 6.1.

Table 6.1: BLDC motor specifications

Type of motor	BLDC motor
Stator voltage	48v
Power rating	250watts
Speed	3500rpm
No. of poles	46
No. of turns 8 Degree	60°

According to the DTC block diagram, the torque and stator flux faults are typically contained within the hysteresis bands. The torque hysteresis band impacts the switching frequency, while the flux hysteresis band primarily affects the stator current distortion in lower-order harmonics. Using two distinct phase currents and the inverter's state, the DTC demands an estimate of the stator flux and torque. One alternative is to estimate flux and torque using two stator phase currents and mechanical speed.

Table 6.2: Space Vectors and Switching States of Inverter

Voltage Vector	Switching States		
	A	B	C
V_0	0	0	0
V_1	1	0	0
V_2	1	1	0
V_3	0	1	0
V_4	0	1	1
V_5	0	0	1
V_6	1	0	1
V_7	1	1	1

The switching logic determines the appropriate voltage vector using torque and flux references. There is no distinction between large and small torque or flux mistakes. Start-up, step changes, and steady-state circumstances all employ the same vectors.

Conclusion

The proposed method, once put into action, generates the firing pulses required to activate the IGBTs in the three-phase fully controlled bridge converter. The tested PWM signals, which are used to operate the BLDC motor's power inverter bridge, were generated using a dsPIC30F4011 Digital Signal Controller. After receiving inputs from the motor's Hall sensors, the proposed system is configured to run at the specified speed. An external potentiometer connected to the microcontroller circuit controls the motor's speed, and the output of the converter is sent to the three-phase stator winding of the 48V, 250 W, 3850 rpm BLDCmmotor. The results show that the program works as intended and that the hardware as designed yields satisfactory results. All requirements of the application were satisfied by the produced control and power circuit. In conclusion, compared to induction and brushed DC motors, BLDC motors are the best. Among these benefits include increased speed ranges, stronger dynamic response, quieter operation, greater efficiency, longer operating life, and enhanced speed versus torque characteristics.

Because of the larger torque supplied to the smaller motor size, it is useful where space and weight are paramount. The consumer goods, appliance, automobile, aerospace, instrumentation, and automation sectors all make extensive use of BLDC motors due to these advantages.

References

1. A. Leonard Marin Florea, "Equational Motors for Electric Vehicle Propulsion: A Comparative Study," in International Scientific Paper Conference, Afases; Brasov, Romania, 2013.
2. K. M. Tan, N. Mithulananthan, and J. Y. Yong, "Ramachandra Murthy, V.K. "A summary of the effects and future possibilities of electric vehicle technology at the cutting edge. Energy Rev," vol. 49, no. 4, pp. 365–385, 2015.
3. L. Mihet-Popa, N. Rao, P. B. Nørgård, and O. M. F. Camacho, "Testing of Battery for Electrical Vehicles in a Distribution Network with Sustainable Energy," IEEE Transactions on Smart Grid, vol. 5, no, 4, pp. 1033–1042, 2014.
4. O. M. Forero Camacho and L. Mihet-Popa, "Fast charging and smart charging tests for electric vehicles batteries using renewable energy," Oil Gas Sci. Technol., vol. 71, no. 1, pp. 1-12, 2016.
5. M. Ehsani, Y. Gao, S. E. Gay, and A. Emadi, "Design and Control Methodology of Plug-in Hybrid Electric Vehicles," IEEE Transactions on Industrial Electronics, vol. 57, no. 2, pp. 633–640, 2010.
6. F. Un-Noor, S. Padmanaban, L. Mihet-Popa, M. Mollah, and E. Hossain, "A comprehensive study of key electric vehicle (EV) components, technologies, challenges, impacts, and future direction of development," Energies, vol. 10, no. 8, p. 1217, 2017.
7. O. M. F. Nørgård, P. B. Rao, and N. Mihet-Popa, "Electrical vehicle batteries tested in a distribution network utilizing sustainable energy," IEEE Transactions on Smart Grid, vol. 5, no. 2, pp. 1033–1042, 2014.
8. D. K. Sharma and R. Tripathi, "4 Intuitionistic fuzzy trigonometric distance and similarity measure and their properties," in Soft Computing, De Gruyter, Berlin, Germany, pp. 53–66, 2020.
9. D. K. Sharma, B. Singh, M. Anam, R. Regin, D. Athikesavan, and M. Kalyan Chakravarthi, "Applications of two separate methods to deal with a small dataset and a high risk of generalization," in 2021 2nd International Conference on Smart Electronics and Communication (ICOSEC), Trichy, India, 2021.
10. B. Senapati and B. S. Rawal, "Adopting a deep learning split-protocol based predictive maintenance management system for industrial manufacturing operations," in Lecture Notes in Computer Science, Singapore: Springer Nature Singapore, pp. 22–39, 2023.
11. B. Senapati and B. S. Rawal, "Quantum communication with RLP quantum resistant cryptography in industrial manufacturing," Cyber Security and Applications, vol. 1, no. 12, p. 100019, 2023.
12. M. A. Yassin et al., "Advancing SDGs : Predicting Future Shifts in Saudi Arabia ' s Terrestrial Water Storage Using Multi-Step-Ahead Machine Learning Based on GRACE Data," 2024.
13. M. A. Yassin, A. G. Usman, S. I. Abba, D. U. Ozsahin, and I. H. Aljundi, "Intelligent learning algorithms integrated with feature engineering for sustainable groundwater salinization modelling: Eastern Province of Saudi Arabia," Results Eng., vol. 20, p. 101434, 2023.

14. S. I. Abba, A. G. Usman, and S. IŞIK, “Simulation for response surface in the HPLC optimization method development using artificial intelligence models: A data-driven approach,” Chemom. Intell. Lab. Syst., vol. 201, no. April, 2020.
15. A. G. Usman et al., “Environmental modelling of CO concentration using AI-based approach supported with filters feature extraction: A direct and inverse chemometrics-based simulation,” Sustain. Chem. Environ., vol. 2, p. 100011, 2023.
16. A. Gbadamosi et al., “New-generation machine learning models as prediction tools for modeling interfacial tension of hydrogen-brine system,” Int. J. Hydrogen Energy, vol. 50, pp. 1326–1337, 2024.
17. I. Abdulazeez, S. I. Abba, J. Usman, A. G. Usman, and I. H. Aljundi, “Recovery of Brine Resources Through Crown-Passivated Graphene, Silicene, and Boron Nitride Nanosheets Based on Machine-Learning Structural Predictions,” ACS Appl. Nano Mater., 2023.
18. S. D. Beedkar, C. N. Khobragade, S. S. Chobe, B. S. Dawane, and O. S. Yemul, "Novel thiazolo-pyrazolyl derivatives as xanthine oxidase inhibitors and free radical scavengers," International Journal of Biological Macromolecules, vol. 50, no. 4, pp. 947-956, 2012.
19. S. S. Chobe, V. A. Adole, K. P. Deshmukh, T. B. Pawar, and B. S. Jagdale, "Poly (ethylene glycol)(PEG-400): A green approach towards synthesis of novel pyrazolo [3, 4-d] pyrimidin-6-amines derivatives and their antimicrobial screening," Archives of Applied Science Research, vol. 6, no. 2, pp. 61-66, 2014.
20. S. S. Chobe, B. S. Dawane, K. M. Tumbi, P. P. Nandekar, and A. T. Sangamwar, "An ecofriendly synthesis and DNA binding interaction study of some pyrazolo [1, 5-a] pyrimidines derivatives," Bioorganic & Medicinal Chemistry Letters, vol. 22, no. 24, pp. 7566-7572, 2012.
21. S. S. Chobe, R. D. Kamble, S. D. Patil, A. P. Acharya, S. V. Hese, O. S. Yemul, and B. S. Dawane, "Green approach towards synthesis of substituted pyrazole-1, 4-dihydro, 9-oxa, 1, 2, 6, 8-tetrazacyclopentano [b] naphthalene-5-one derivatives as antimycobacterial agents," Medicinal Chemistry Research, vol. 22, pp. 5197-5203, 2013.
22. H. A. Al-Asadi, M. H. Al-Mansoori, M. Ajiya, S. Hitam, M. I. Saripan, and M. A. Mahdi, “Effects of pump recycling technique on stimulated Brillouin scattering threshold: A theoretical model,” Optics Express, vol. 18, no. 21, pp. 22339- 22347, 2010.
23. H. A. Al-Asadi, M. H. Al-Mansoori, M. I. Saripan, and M. A. Mahdi, “Brillouin Linewidth Characterization in Single Mode Large Effective Area Fiber through the Co-Pumped Technique,” International Journal of Electronics, Computer and Communications Technologies (IJECCT), vol. 1, no. 1, pp. 16-20, 2010.
24. H. A. Al-Asadi, M. H. Al-Mansoori, S. Hitam, M. I. Saripan, and M. A. Mahdi, “Particle swarm optimization on threshold exponential gain of stimulated Brillouin scattering in single mode fibers,” Optics Express, vol. 19, no. 3, pp. 1842-1853, 2011.
25. H. A. Al-Asadi, M. H. Al-Mansoori, S. Hitam, M. I. Saripan, and M. A. Mahdi, “Analytical study of nonlinear phase shift through stimulated Brillouin scattering in single mode fibre with pump power recycling technique,” Journal of Optics, vol. 13 no. 10, 2011.
26. H. A. Al-Asadi, M. H. Abu Bakar, M. H. Al-Mansoori, F. R. Mahamd Adikan, and M. A. Mahdi, “Analytical analysis of second-order Stokes wave in Brillouin ring fiber laser,” Optics. Express, vol. 19, no. 25, pp. 25741- 25748, 2011.
27. M. Al-Asadi, Y. A. Al-Asadi, and H. A. Al-Asadi, “Architectural Analysis of Multi-Agents Educational Model in Web-Learning Environments,” Journal of Emerging Trends in Computing and Information Sciences, vol. 3, no. 6, 2012.

28. M. A. Abed and H. A. Al-Asadi, “Simplifying Handwritten Characters Recognition Using a Particle Swarm Optimization Approach,” European Academic Research, vol 1, pp. 535- 552, 2013.

29. M. A. Abed and H. A. Al-Asadi, “High Accuracy Arabic Handwritten Characters Recognition using (EBPANN) Architecture,” International Journal of Advanced Computer Science and Applications (IJACSA), vol. 6, no. 2, pp. 145-152, 2015.

30. H. A. Al-Asadi and M. A. Abed, “Object Recognition Using Artificial Fish Swarm Algorithm on Fourier Descriptors,” American Journal of Engineering, Technology and Society, vol 2, no. 5, pp. 105-110, 2015.

31. B. S. Dawane, S. G. Konda, N. T. Khandare, S. S. Chobe, B. M. Shaikh, R. G. Bodade, and V. D. Joshi, "Synthesis and antimicrobial evaluation of 2-(2-butyl-4-chloro-1H-imidazol-5-yl-methylene)-substituted-benzofuran-3-ones," Organic Communications, vol. 3, no. 2, pp. 22, 2010.

32. B. S. Dawane, S. G. Konda, B. M. Shaikh, S. S. Chobe, N. T. Khandare, V. T. Kamble, and R. B. Bhosale, "Synthesis and in vitro antimicrobial activity of some new 1-thiazolyl-2-pyrazoline derivatives," Synthesis, vol. 1, no. 009, 2010.

33. B. S. Dawane, B. M. Shaikh, N. T. Khandare, V. T. Kamble, S. S. Chobe, and S. G. Konda, "Eco-friendly polyethylene glycol-400: a rapid and efficient recyclable reaction medium for the synthesis of thiazole derivatives," Green Chemistry Letters and Reviews, vol. 3, no. 3, pp. 205-208, 2010.

34. M. Haroun, S. S. Chobe, R. R. Alavala, S. M. Mathure, R. N. Jamullamudi, C. K. Nerkar, and M. K. Anwer, "1, 5-benzothiazepine derivatives: green synthesis, in silico and in vitro evaluation as anticancer agents," Molecules, vol. 27, no. 12, pp. 3757, 2022.

35. S. A. Shaikh, S. R. Labhade, R. R. Kale, P. Y. Pachorkar, R. J. Meshram, K. S. Jain, and D. R. Boraste, "Thiadiazole-Thiazole Derivatives as Potent Anti-Tubercular Agents: Synthesis, Biological Evaluation, and In Silico Docking Studies," European Journal of Medicinal Chemistry Reports, vol. 100183, 2024.

36. S. A. Shaikh, S. R. Labhade, R. R. Kale, P. Y. Pachorkar, R. J. Meshram, K. S. Jain, and S. N. Wakchaure, "Synthesis, Biological and Molecular Docking Studies of Thiazole-Thiadiazole derivatives as potential Anti-Tuberculosis Agents," Chemistry & Biodiversity, vol. 21, no. 6, e202400496, 2024.

37. P. Sonawane, C. L. Ladekar, G. A. Badiger, and R. A. Deore, "Design and analysis of serviceable cantilever fit snap in automotive plastic parts," World Journal of Engineering, vol. ahead-of-print, no. ahead-of-print, 2024.

38. P. R. Sonawane, D. M. Deshmukh, A. Gajbhiye, et al., "An investigation into the mechanical properties of an epoxy-based composite made from jute fiber and reinforced with Sal tree gum powder," Journal of the Institution of Engineers (India): Series D, vol. 105, pp. 665–674, 2024.

39. A. M. Gajbhiye, P. R. Sonawane, A. H. Karle, et al., "Optimization of welding parameters for En8D and SAE1018 materials by Taguchi," International Journal on Interactive Design and Manufacturing, 2023.

40. B. S. Alotaibi et al., “Sustainable Green Building Awareness: A Case Study of Kano Integrated with a Representative Comparison of Saudi Arabian Green Construction,” Buildings, vol. 13, no. 9, 2023.

41. S. I. Abba et al., “Integrated Modeling of Hybrid Nanofiltration/Reverse Osmosis Desalination Plant Using Deep Learning-Based Crow Search Optimization Algorithm,” Water (Switzerland), vol. 15, no. 19, 2023.

42. S. I. Abba, J. Usman, and I. Abdulazeez, “Enhancing Li + recovery in brine mining : integrating next-gen emotional AI and explainable ML to predict adsorption energy in crown ether-based hierarchical nanomaterials,” pp. 15129–15142, 2024.
43. J. Usman, S. I. Abba, N. Baig, N. Abu-Zahra, S. W. Hasan, and I. H. Aljundi, “Design and Machine Learning Prediction of In Situ Grown PDA-Stabilized MOF (UiO-66-NH2) Membrane for Low-Pressure Separation of Emulsified Oily Wastewater,” ACS Appl. Mater. Interfaces, Mar. 2024.
44. B. Senapati et al., “Wrist crack classification using deep learning and X-ray imaging,” in Proceedings of the Second International Conference on Advances in Computing Research (ACR’24), Cham: Springer Nature Switzerland, pp. 60–69, 2024.
45. A. B. Naeem et al., “Heart disease detection using feature extraction and artificial neural networks: A sensor-based approach,” IEEE Access, vol. 12, no.3, pp. 37349–37362, 2024.
46. R. Tsarev et al., “Automatic generation of an algebraic expression for a Boolean function in the basis ∧, ∨, ¬,” in Data Analytics in System Engineering, Cham: Springer International Publishing, Switzerland, pp. 128–136, 2024.
47. R. Tsarev, B. Senapati, S. H. Alshahrani, A. Mirzagitova, S. Irgasheva, and J. Ascencio, “Evaluating the effectiveness of flipped classrooms using linear regression,” in Data Analytics in System Engineering, Cham: Springer International Publishing, Switzerland, pp. 418–427, 2024.
48. D. K. Sharma, B. Singh, M. Anam, K. O. Villalba-Condori, A. K. Gupta, and G. K. Ali, “Slotting learning rate in deep neural networks to build stronger models,” in 2021 2nd International Conference on Smart Electronics and Communication (ICOSEC), Trichy, India, 2021.
49. K. Kaliyaperumal, A. Rahim, D. K. Sharma, R. Regin, S. Vashisht, and K. Phasinam, “Rainfall prediction using deep mining strategy for detection,” in 2021 2nd International Conference on Smart Electronics and Communication (ICOSEC), Trichy, India, 2021.
50. I. Nallathambi, R. Ramar, D. A. Pustokhin, I. V. Pustokhina, D. K. Sharma, and S. Sengan, “Prediction of influencing atmospheric conditions for explosion Avoidance in fireworks manufacturing Industry-A network approach,” Environ. Pollut., vol. 304, no. 7, p. 119182, 2022.
51. H. Sharma and D. K. Sharma, “A Study of Trend Growth Rate of Confirmed Cases, Death Cases and Recovery Cases of Covid-19 in Union Territories of India,” Turkish Journal of Computer and Mathematics Education, vol. 13, no. 2, pp. 569–582, 2022.
52. A. L. Karn et al., “Designing a Deep Learning-based financial decision support system for fintech to support corporate customer’s credit extension,” Malays. J. Comput. Sci., vol.36, no.s1, pp. 116–131, 2022.
53. A. L. Karn et al., “B-lstm-Nb based composite sequence Learning model for detecting fraudulent financial activities,” Malays. J. Comput. Sci., vol.32, no.s1, pp. 30–49, 2022.
54. P. P. Dwivedi and D. K. Sharma, “Application of Shannon entropy and CoCoSo methods in selection of the most appropriate engineering sustainability components,” Cleaner Materials, vol. 5, no. 9, p. 100118, 2022.
55. A. Kumar, S. Singh, K. Srivastava, A. Sharma, and D. K. Sharma, “Performance and stability enhancement of mixed dimensional bilayer inverted perovskite (BA2PbI4/MAPbI3) solar cell using drift-diffusion model,” Sustain. Chem. Pharm., vol. 29, no. 10, p. 100807, 2022.
56. A. Kumar, S. Singh, M. K. A. Mohammed, and D. K. Sharma, “Accelerated innovation in developing high-performance metal halide perovskite solar cell using machine learning,” Int. J. Mod. Phys. B, vol. 37, no. 07, p.12, 2023.

57. G. A. Ogunmola, M. E. Lourens, A. Chaudhary, V. Tripathi, F. Effendy, and D. K. Sharma, “A holistic and state of the art of understanding the linkages of smart-city healthcare technologies,” in 2022 3rd International Conference on Smart Electronics and Communication (ICOSEC), Trichy, India, 2022.

58. P. Sindhuja, A. Kousalya, N. R. R. Paul, B. Pant, P. Kumar, and D. K. Sharma, “A Novel Technique for Ensembled Learning based on Convolution Neural Network,” in 2022 International Conference on Edge Computing and Applications (ICECAA), IEEE, Tamil Nadu, India, pp. 1087–1091, 2022.

59. A. R. B. M. Saleh, S. Venkatasubramanian, N. R. R. Paul, F. I. Maulana, F. Effendy, and D. K. Sharma, “Real-time monitoring system in IoT for achieving sustainability in the agricultural field,” in 2022 International Conference on Edge Computing and Applications (ICECAA), Tamil Nadu, India, 2022.

60. Srinivasa, D. Baliga, N. Devi, D. Verma, P. P. Selvam, and D. K. Sharma, “Identifying lung nodules on MRR connected feature streams for tumor segmentation,” in 2022 4th International Conference on Inventive Research in Computing Applications (ICIRCA), Tamil Nadu, India, 2022.

61. C. Goswami, A. Das, K. I. Ogaili, V. K. Verma, V. Singh, and D. K. Sharma, “Device to device communication in 5G network using device-centric resource allocation algorithm,” in 2022 4th International Conference on Inventive Research in Computing Applications (ICIRCA), Tamil Nadu, India , 2022.

62. M. Yuvarasu, A. Balaram, S. Chandramohan, and D. K. Sharma, “A Performance Analysis of an Enhanced Graded Precision Localization Algorithm for Wireless Sensor Networks,” Cybernetics and Systems, pp. 1–16, 2023, Press.

63. P. P. Dwivedi and D. K. Sharma, “Evaluation and ranking of battery electric vehicles by Shannon’s entropy and TOPSIS methods,” Math. Comput. Simul., vol. 212, no.10, pp. 457–474, 2023.

64. P. P. Dwivedi and D. K. Sharma, “Assessment of Appropriate Renewable Energy Resources for India using Entropy and WASPAS Techniques,” Renewable Energy Research and Applications, vol. 5, no. 1, pp. 51–61, 2024.

65. P. P. Dwivedi and D. K. Sharma, “Selection of combat aircraft by using Shannon entropy and VIKOR method,” Def. Sci. J., vol. 73, no. 4, pp. 411–419, 2023.

66. Z. H. Ahmed, A. S. Hameed, M. L. Mutar, and H. Haron, "An Enhanced Ant Colony System Algorithm Based on Subpaths for Solving the Capacitated Vehicle Routing Problem," Symmetry, vol. 15, no. 11, p. 2020, 2023.

67. M. L. Mutar, A. Burhanuddin, S. Hameed, N. Yusof, M. F. Alrifaie, and A. A. Mohammed, "Multi-objectives ant colony system for solving multi-objectives capacitated vehicle routing problem," Journal of Theoretical and Applied Information Technology, vol. 98, no. 24, 2020.

68. M. F. Alrifaie, Z. H. Ahmed, A. S. Hameed, and M. L. Mutar, "Using machine learning technologies to classify and predict heart disease," International Journal of Advanced Computer Science and Applications, vol. 12, no. 3, 2021.

69. A. S. Hameed, B. M. Aboobaider, N. H. Choon, M. L. Mutar, and W. H. Bilal, "Review on the methods to solve combinatorial optimization problems particularly: quadratic assignment model," International Journal of Engineering & Technology, vol. 7, no. 3.20, pp. 15–20, 2018.

70. M. L. Mutar, B. M. Aboobaider, and A. S. Hameed, "Rev Vehicle Routing Problem and Future Research Trend," International Journal of Applied Engineering Research, vol. 12, no. 20, 2017.

71. F. A. O. Sari et al., "Networks cyber security model by using machine learning techniques," International Journal of Intelligent Systems and Applications in Engineering, vol. 10, no. 1, pp. 257–263, 2022.
72. M. F. Alrifaie, O. A. Ismael, A. S. Hameed, and M. B. Mahmood, "Pedestrian and objects detection by using learning complexity-aware cascades," in Proc. 2021 2nd Information Technology To Enhance e-Learning and Other Application (IT-ELA), pp. 12–17, IEEE, Dec. 2021.
73. G. Kashyap, "Unsupervised learning for high-dimensional data: Advancements in unsupervised learning techniques like clustering, anomaly detection, and dimensionality reduction," Int. J. Leading Res. Publ., vol. 5, no. 12, pp. 1–10, Dec. 2024.
74. G. Kashyap, "Meta-learning: Learning to learn: Investigating how meta-learning algorithms can improve learning efficiency across tasks," Int. J. Sci. Res. Eng. Manag., vol. 8, no. 12, pp. 1–7, Dec. 2024.
75. G. Kashyap, "Infrastructure automation using Ansible and YAML for IT environment build in the health insurance industry," Int. J. Innov. Res. Creat. Technol., vol. 10, no. 6, pp. 1–10, Dec. 2024.
76. G. Kashyap, "Quantum machine learning: Exploring the intersection of quantum computing and AI," Int. J. Innov. Res. Eng. Multidiscip. Phys. Sci., vol. 13, no. 2, pp. 1–8, Mar.–Apr. 2025.
77. G. Kashyap, "AI for robustness and fairness: Addressing bias, fairness, and robustness in machine learning algorithms," Sci. Data Learn. Mach. Intell. Artif. J., vol. 1, no. 3, pp. 1–15, Jan. 2025.
78. A. S. Hameed, B. M. Aboobaider, H. C. Ngo, and M. L. Mutar, "Improved discrete differential evolution algorithm in solving quadratic assignment problem for best solutions," International Journal of Advanced Computer Science and Applications, vol. 9, no. 12, 2018.
79. A. A. Khudhair et al., "Impact on Higher Education and College Students in Dijlah University after COVID through E-learning," Computer-Aided Design and Applications, pp. 104–115, 2023.
80. A. S. Hameed et al., "A hybrid method integrating a discrete differential evolution algorithm with tabu search algorithm for the quadratic assignment problem: A new approach for locating hospital departments," Mathematical Problems in Engineering, vol. 2021, no. 1, p. 6653056, 2021.
81. A. T. Jalil et al., "Analytical model for thermoelastic damping in in-plane vibrations of circular cross-sectional micro/nanorings with dual-phase-lag heat conduction," Journal of Vibration Engineering & Technologies, vol. 12, no. 1, pp. 797–810, 2024.
82. A. S. Hameed, B. M. Aboobaider, N. H. Choon, M. L. Mutar, and W. H. Bilal, "A comparative study between the branch and cut algorithm and ant colony algorithm to solve the electric meter reader problem in rural areas," Opcion, vol. 34, no. 86, pp. 1525–1539, 2018.